Rare Metal Materials and Engineering
Volume 49, Issue 9, September 2020
Available online at www.rmme.ac.cn

Science Press

Cite this article as: Rare Metal Materials and Engineering, 2020, 49(9): 2956-2965.

ARTICLE

Hot Deformation Behavior and Hot Processing Map of GH2907 Superalloy

Chen Yizhe[1,2], Pang Yuhua[1,2], Wang Jianguo[3], Liu Dong[3], Wang Jianyan[4]

[1] Xi'an University of Architecture and Technology, Xi'an 710055, China; [2] Shaanxi Province Metallurgical Engineering Technology Research Center, Xi'an 710055, China; [3] Northwestern Polytechnical University, Xi'an 710072, China; [4] China Aerospace Shenyang Dawn Aviation Engine (Group) Co., Ltd, Shenyang 110000, China

Abstract: The hot deformation behavior of GH2907 superalloy at deformation temperature of 950~1100 °C, strain rates of 0.01~10 s^{-1} and deformation degree of 60% was studied by thermal simulation compression experiments. The results show that flow stress decreases significantly as the deformation temperature increases or strain rate decreases; according to the Arrhenius equation and the Zener-Hollomon parameter, the thermal deformation activation energy (Q) can be calculated, and the hot deformation constitutive equation of GH2907 superalloy is also established. On the basis of the dynamic material model, the power dissipation map under different strains of the GH2907 superalloy is obtained. The region with higher power dissipation efficiency (η) is located at the temperature of 1050~1100 °C and strain rates of 0.01~0.03 s^{-1}, and the microstructure dynamic recrystallization phenomenon also occurs in the deformation region; based on the Prasad instability criterion, the hot processing map of GH2907 superalloy under different strains is drawn. The rheological instability zone is located in the high temperature range of 970~1100 °C and high strain rate range of 0.6~10 s^{-1}. In addition, the dynamic recrystallized grains are distributed along the adiabatic shear band and flow locally in this deformation region. According to the hot processing map and microstructure analysis of GH2907 superalloy, the suitable processing area is in the temperature range of 1050~1100 °C and strain rates of 0.01~0.03 s^{-1}.

Key words: GH2907 superalloy; hot deformation behavior; hot processing map; power dissipation efficiency; instability criterion

It is very essential to study the hot deformation behavior and hot workability of GH2907 superalloy at high temperature for the development of reasonable forging and ring rolling processes. The constitutive relationship is usually used to describe the plastic rheological properties of metals, which can reflect the influence of factors such as microstructure evolution and process parameters on the flow stress, and also show the thermal deformation characteristics of the alloy [1]. The hot processing map is an effective tool to control the microstructure of metallic materials during thermal deformation and to optimize the forming process parameters [2]. Much useful information can be obtained through the hot processing map, such as the optimal process parameters of the metallic material in the process of hot deformation, the predictable rheological instability process parameters that may occur during the deformation process, and the reasonable instability deformation mechanism of the alloy [3].

In this study, the hot deformation behavior of GH2907 superalloy was analyzed by thermal simulation compression experiments; the thermal deformation constitutive equation of the alloy was established; the power dissipation map of the alloy under different strains was obtained according to the dynamic material model (DMM) and the optimum process parameters of deformation can also be determined; based on the Prasad instability criterion, the hot processing map of the superalloy under different strains was drawn to predict the rheological instability process parameters that

Received date: September 01, 2019
Foundation item: National Natural Science Foundation of China (51504195); Key R&D Program Projects in Shaanxi Province (2017ZDXM-GY-027)
Corresponding author: Chen Yizhe, Candidate for Master, School of Metallurgical Engineering, Xi'an University of Architecture and Technology, Xi'an 710055, P. R. China, E-mail: 957698190@qq.com

may occur during the deformation process. Combined with the analysis of the structure, the instability deformation mechanism of the superalloy during the hot deformation process can be obtained.

1 Experiment

The material used in this experiment was GH2907 superalloy forged bar, the chemical composition of which is shown in Table 1, and the thermal simulated compression sample of Φ8 mm×12 mm was cut. The microstructure after solid solution treatment at 1030 °C for 30 min before deformation is shown in Fig.1. The microstructure is uniform and the average grain size is about 75 μm. Axial near isothermal compression experiments were performed on a Gleeble-3500 thermal simulator at the deformation temperatures of 950, 1000, 1050 and 1100 °C and strain rates of 0.01, 0.1, 1 and 10 s^{-1}. The compression deformation degree was 60% with the heating rate of 10 °C/s and the holding time of 10 min. Graphite sheets were adhered to both ends of the sample before hot compression, and water quenching was performed immediately after the thermal compression to preserve the microstructure. The shapes of the sample before and after deformation are shown in Fig.2. The deformed sample was cut along the compression axis, and then etched with a mixed solution of HCl (50 mL)+CH_3CH_2OH (50 mL)+$FeCl_3$ (45 g)+H_2O (40 mL)+HF (15 mL) after grinding and polishing at room temperature. Finally, the microstructure of the superalloy was observed by LWD300LT optical microscope.

2 Results and Discussion

2.1 True stress-true strain curves of GH2907 superalloy

The true stress-true strain curve of GH2907 superalloy under different deformation temperatures and strain rates is shown in Fig.3. It can be seen that the flow stress of the superalloy decreases significantly as the deformation temperature increases or strain rate decreases. The curves show the trend of hardening first and then softening under different deformation conditions, and also present obvious dynamic recrystallization characteristics. In the initial stage of deformation, the generation and proliferation of dislocations can contribute to the rapid increase in the dislocation density, a sharp increase in flow stress and the obvious work hardening effect. Besides, the small softening effect of dynamic recovery results in an increase in flow stress as the strain increases [4]. With the increase of strain, the dynamic softening mechanism is gradually enhanced, and the rising rate of flow stress slows down until the peak stress is reached. The softening rate caused by DRV and DRX is larger than the work hardening rate, and the flow stress is gradually reduced [5]. As the amount of deformation increases, dynamic softening and work hardening eventually reach dynamic equilibrium. In addition, the flow stress tends to be stable, which leads to the steady-state stress stage.

At the same strain rate, the flow stress decreases as the deformation temperature increases. In addition, the thermal activation energy of the superalloy is enhanced due to the deformation temperature rise, which helps shorten the incubation period of the dynamic recovery and increase dynamic recrystallization nucleation rate and the growth rate of the crystal grains, and finally these factors result in the enhanced softening effect caused by recrystallization [6]. At the same deformation temperature, the flow stress decreases as the strain rate decreases. The increasing deformation temperature leads to the increasing amplitude of the atomic thermal motion, the decreasing interaction force between the atoms, the reduced slip resistant force and the increas-

Table 1 Chemical composition of GH2907 superalloy (wt%)

C	Mn	Si	Cr	Ni	S	P	Al	Ti	Cu	Co	B	Nb+Ta	Mo	Fe
0.028	0.49	0.33	0.058	37.83	0.0024	0.0060	0.016	1.71	0.021	14.13	0.0067	4.91	0.0032	40.4587

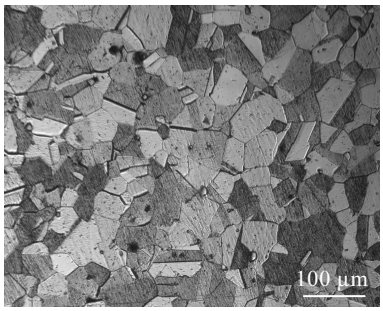

Fig.1 Original microstructure of GH2907 superalloy sample

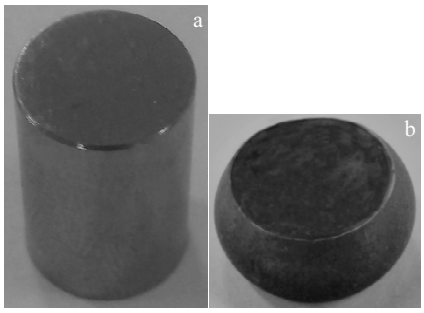

Fig.2 Shape of GH2907 superalloy sample before (a) and after (b) deformation

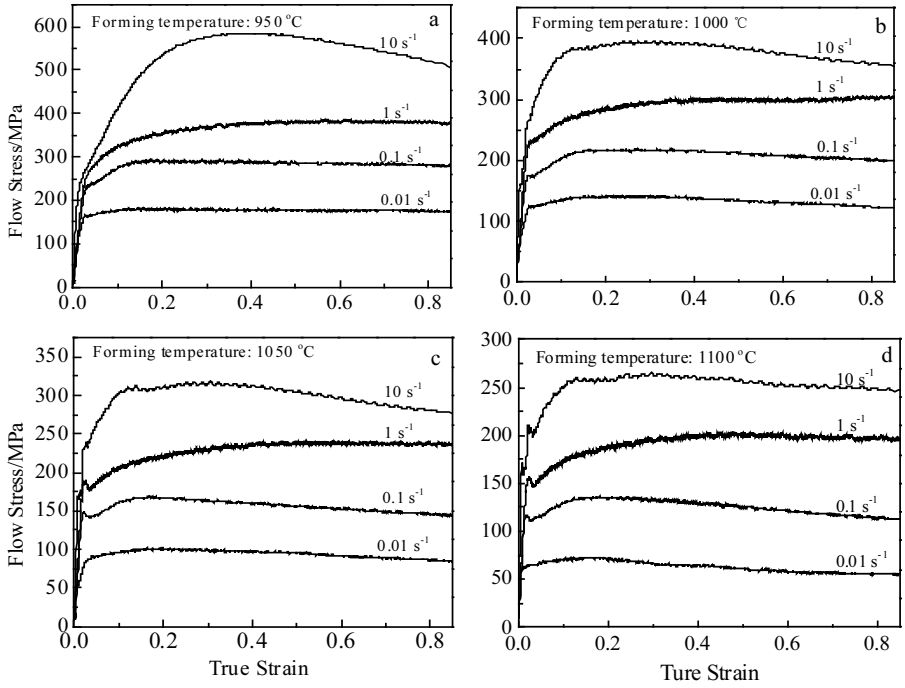

Fig.3 True stress-strain curves of GH907 superalloy under different deformation conditions: (a) 950 °C, (b) 1000 °C, (c) 1050 °C, and (d) 1100 °C

ing deformation slip system, which is beneficial to the deformation of the material [7]. The dynamic recrystallization nucleation and growth as well as dislocation motion (including slip, cross slip and climb) need longer time due to the lower strain rate, which results in fully completed recrystallization and evident softening during deformation [8].

At high strain rate, the flow stress curve shows sawtooth fluctuations, especially when the strain rate is 10 s^{-1}, and the true stress-true strain curve at each deformation temperature has a larger fluctuation range. During the thermal deformation process of the superalloy, there is a discontinuous dynamic recrystallization phenomenon, which leads to a rapid increase in storage energy until the driving force required for dynamic recrystallization is reached [9]. After the occurrence of dynamic recrystallization, there is sufficient time for the softening phenomenon caused by dynamic recrystallization and work hardening phenomenon to reach a dynamic balance.

2.2 Constitutive equation of GH2907 superalloy

The total effect of strain rate and deformation temperature on the flow stress of the superalloy can be characterized by the Zener-Hollomon parameter [10]:

$$Z = \dot{\varepsilon}\exp(Q/RT) \quad (1)$$

where $\dot{\varepsilon}$ is the strain rate (s^{-1}), σ is the flow stress (MPa), T is the absolute temperature (K), R is the general gas constant (R=8.3145 J·mol^{-1}·K^{-1}), Q is thermal deformation activation energy (J·mol^{-1}).

The hot deformation process of the superalloy is a thermal activation process, and three different forms of Arrhenius equation are usually applied to analyze the relationship among σ, $\dot{\varepsilon}$ and T [11]:

$$\dot{\varepsilon} = A_1\sigma^{n_1}\exp(-Q/RT) \quad (2)$$

$$\dot{\varepsilon} = A_2\exp(\beta\sigma)\exp(-Q/RT) \quad (3)$$

$$\dot{\varepsilon} = A\left[\sinh(\alpha\sigma)\right]^n\exp(-Q/RT) \quad (4)$$

where A_1, A_2, A, n_1, α and β are all temperature independent constants, and n is a parameter related to the strain rate sensitivity index. Eq.(2~4) are the exponential equation, the power equation and the hyperbolic sine equation of the Arrhenius equation, respectively. Then the relationship among α, n_1 and β can be expressed:

$$\alpha = \beta/n_1 \quad (5)$$

The exponential equation and the power equation of the Arrhenius equation are suitable for low stress and high stress conditions, respectively, and the Arrhenius hyperbolic sine equation is applicable to the hot deformation process in a wider stress range. Since the accuracy of flow stress is greatly affected by the measurement accuracy, in order to describe the high temperature deformation characteristics of the superalloy, the peak stress data is used to construct the constitutive relation [12]. The peak stress (σ_p) under different deformation conditions can be measured by the corresponding true stress-strain curve. The expression can be

obtained after taking the logarithm from each side of Eq.(2~4):

$$\ln\sigma = \frac{1}{n_1}\ln\dot{\varepsilon} + \frac{1}{n_1}\left(\frac{Q}{RT} - \ln A_1\right) \quad (6)$$

$$\sigma = \frac{1}{\beta}\ln\dot{\varepsilon} + \frac{1}{\beta}\left(\frac{Q}{RT} - \ln A_2\right) \quad (7)$$

$$\ln\left[\sinh(\alpha\sigma)\right] = \frac{1}{n}(\ln\dot{\varepsilon}) + \frac{Q}{nRT} - \frac{\ln A}{n} \quad (8)$$

The values of n_1 and β are calculated using the relationship between the peak stress (σ_p) in Eq.(6) and Eq.(7). As shown in Fig.4 and Fig.5, the relationship between lnσ and $\ln\dot{\varepsilon}$ as well as σ and $\ln\dot{\varepsilon}$, respectively, is obtained by linear regression fitting using the least squares method to obtain the slope: n_1=6.1601 and β=0.0265 MPa^{-1}. The value of α at different deformation temperatures is obtained from Eq.(5), and the average value of α is 0.0043 MPa^{-1}.

When T is constant, ln[sinh($\alpha\sigma$)] and $\ln\dot{\varepsilon}$ are linear, and the fitted ln[sinh($\alpha\sigma$)]-$\ln\dot{\varepsilon}$ line is shown in Fig.6. The average value of the slope 1/n is 0.2201. When $\dot{\varepsilon}$ is constant, ln[sinh($\alpha\sigma$)] and 1/T are linear, and the fitted ln[sinh($\alpha\sigma$)]-1/T line is shown in Fig.7. The average value of the slope Q/(nR) is 12 259.9628.

It can be seen from the figure that the flow stress satisfies Eq.(8), and after the deformation of Eq.(8), the expression can be obtained by taking partial differential from two sides:

$$Q = R\left|\frac{\partial In\dot{\varepsilon}}{\partial\ln\left[\sinh(\alpha\sigma)\right]}\right|_T\left|\frac{\partial\ln\left[\sinh(\alpha\sigma)\right]}{\partial(1/T)}\right|_{\dot{\varepsilon}} \quad (9)$$

The first partial differentials on the right sides of Eq.(9) is the reciprocal of the slope of ln[sinh($\alpha\sigma$)]-$\ln\dot{\varepsilon}$ relationship at a certain deformation temperature, that is, the mean value of n is 4.5425; besides, the second differential is the mean value [Q/(nR)] of the slope of the ln[sinh($\alpha\sigma$)]-1/T relationship at a constant strain rate, and the value is 12 259.9628. The thermal deformation activation energy (Q) of the GH2907 superalloy was calculated to be 463.043 kJ·mol^{-1} by substituting these two slope values and the R value of 8.3145 J·mol^{-1}·K^{-1} into Eq.(9).

Substituting Eq.(1) into Eq.(4), and finding the logarithm on both sides of the equation:

$$\ln[\sinh(\alpha\sigma)] = \frac{\ln Z}{n} - \frac{\ln A}{n} \quad (10)$$

Based on the obtained Q value, the Z value under the corresponding deformation condition is calculated. It can be seen from Eq.(10) that ln[sinh($\alpha\sigma$)] and ln$Z$ have a linear relationship with a slope of 1/n and an intercept of ln(A/n). The ln[sinh($\alpha\sigma$)]-ln$Z$ relationship curve is shown in Fig.8. The average value of ln(A/n) is calculated to be 9.0255, and the value of A is 6.3876×10^{17}.

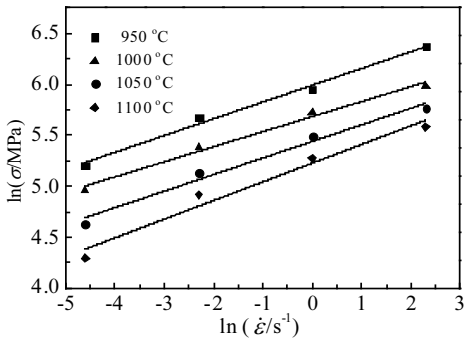

Fig.4 Relationship diagrams between lnσ and $\ln\dot{\varepsilon}$

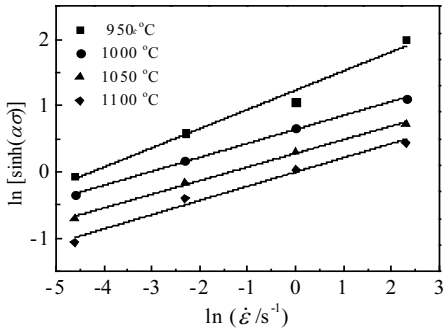

Fig.6 Correlation diagrams between ln[sinh($\alpha\sigma$)] and $\ln\dot{\varepsilon}$

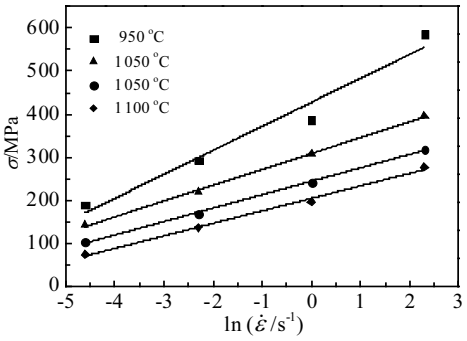

Fig.5 Relationship diagrams between σ and $\ln\dot{\varepsilon}$

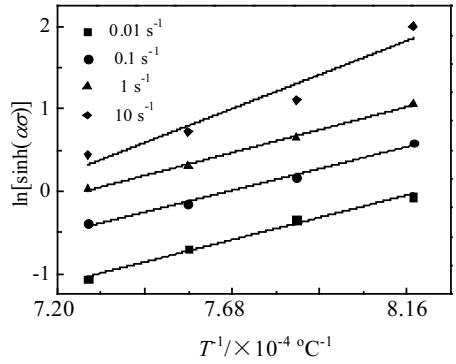

Fig.7 Correlation diagrams between ln[sinh($\alpha\sigma$)] and 1/T

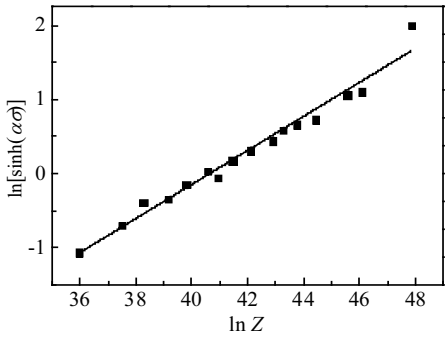

Fig.8 Relation diagrams between ln[sinh($\alpha\sigma$)] and ln$Z$

Therefore, the hyperbolic sine function equation is used to characterize the relationship among σ_p, T and $\dot{\varepsilon}$ of the GH2907 superalloy:

$$\dot{\varepsilon} = 6.3876\times10^{17}\left[\sinh\left(0.0043\sigma\right)\right]^{4.5425}\exp\left[-\frac{463043}{8.3145T}\right] \quad (11)$$

The equation is applicable to the hot deformation behavior of GH2907 superalloy at the deformation temperatures of 950~1100 °C and strain rates of 0.01~10 s^{-1}.

2.3 Hot processing map of GH2907 superalloy

2.3.1 Power dissipation map of GH2907 superalloy

Under certain deformation temperature and strain conditions, the influence of the corresponding deformation rate of metal materials during thermal deformation can be described by constitutive equations [13]:

$$\sigma = K\dot{\varepsilon}^m \quad (12)$$

where σ is the flow stress, $\dot{\varepsilon}$ is the strain rate, K is the material constant and m is the strain rate sensitivity index. According to the DMM model, the thermally deformed workpiece is a nonlinear energy dissipating unit, in which the energy (P) of the input workpiece can be decomposed into two parts: dissipator content (G) and dissipator co-content (J) [14]:

$$P = \sigma\dot{\varepsilon} = G + J = \int_0^{\dot{\varepsilon}}\varepsilon \mathrm{d}\dot{\varepsilon} + \int_0^{\sigma}\dot{\varepsilon}\mathrm{d}\sigma \quad (13)$$

where G refers to the power consumption during thermal deformation of the material; J refers to the power consumption during the evolution of material during thermal deformation [15]:

$$G = \int_0^{\dot{\varepsilon}}\varepsilon \mathrm{d}\dot{\varepsilon} = \frac{\sigma\dot{\varepsilon}}{1+m} \quad (14)$$

$$J = \int_0^{\sigma}\dot{\varepsilon}\mathrm{d}\sigma = \frac{m\sigma\dot{\varepsilon}}{m+1} \quad (15)$$

The relationship between G and J can be determined by the strain rate sensitivity index (m) [16]:

$$m = \frac{\partial J}{\partial G} = \left(\frac{\partial \ln\sigma}{\partial \ln\dot{\varepsilon}}\right)_{T,\dot{\varepsilon}} \quad (16)$$

The value range of m is from 0 to 1 for steady-state rheology of viscoplastic solids. In addition, the larger the value, the greater the dissipativeness of the corresponding microstructure. When the material system is considered to be an ideal linear power dissipation (m=1), and J reaches its maximum (J_{max}), Eq.(17) can be obtained:

$$J_{max} = \frac{\sigma\dot{\varepsilon}}{2} \quad (17)$$

For the nonlinear power dissipation, the power dissipation efficiency caused by the microstructure evolution is expressed through the power dissipation efficiency (η):

$$\eta = \frac{J}{J_{max}} = \frac{2m}{m+1} \quad (18)$$

η is a function of ε, $\dot{\varepsilon}$ and T which varies with the change of $\dot{\varepsilon}$ and T; besides, it means the ratio of the power dissipated by the microstructure evolution to the linear dissipative power of the material during deformation [17]. The higher η value corresponds to the better processing performance area, and the mechanism of metal material microstructure evolution in the process of thermal deformation can be preliminarily judged according to the power dissipation map.

Solas et al[18] used cubic spline interpolation to fit the relationship between $\ln\sigma$ and $\ln\dot{\varepsilon}$, and the relevant derivative calculation is carried out with the curve calculated by this method. The relationship between $\ln\sigma$ and $\ln\dot{\varepsilon}$ which is established by the cubic spline interpolation function can be described as follows:

$$\ln\sigma = a_1 + a_2\ln\dot{\varepsilon} + a_3\left(\ln\dot{\varepsilon}\right)^2 + a_4\left(\ln\dot{\varepsilon}\right)^3 \quad (19)$$

The least squares cubic polynomial fitting is applied to the data, and the values of the coefficients a_1, a_2, a_3, and a_4 of the polynomial are obtained by regression. The strain rate sensitivity index m is calculated by deriving $\ln\dot{\varepsilon}$ on both sides of Eq.(19):

$$m = a_2 + 2a_3\ln\dot{\varepsilon} + 3a_4\left(\ln\dot{\varepsilon}\right)^2 \quad (20)$$

The value of m is obtained by substituting the value of a under different deformation conditions into Eq.(20), and the power dissipation efficiency (η) is gained by substituting the calculated value of m into Eq.(21):

$$\eta = \frac{2[a_2 + 2a_3\ln\dot{\varepsilon} + 3a_4\left(\ln\dot{\varepsilon}\right)^2]}{a_2 + 2a_3\ln\dot{\varepsilon} + 3a_4\left(\ln\dot{\varepsilon}\right)^2 + 1} \quad (21)$$

Fig.9 is the power dissipation map of GH2907 superalloy under different strains during hot deformation. When the strain is 0.1, the minimum value of η is in the temperature range 950~1100 °C and the strain rate range 0.14~1.65 s^{-1}; the maximum value of η is located in the temperature range 950~1100 °C and the strain rate range 0.01~0.03 s^{-1}, as well as 1020~1100 °C and 6.05~10 s^{-1}. As the strain increases, the region of minimum η moves to the upper right corner, and the region of maximum η moves to the lower right corner. When the strain reaches 0.7, the region of minimum η is in

the temperature range 950~1000 °C and the strain rate range 0.08~4.48 s^{-1}, as well as 1000~1100 °C and 0.6~10 s^{-1}. The maximum value of η is located in the temperature range 950~980 °C and the strain rate range 0.01~0.03 s^{-1}, as well as 1020~1100 °C and 0.01~0.16 s^{-1}. The η value increases as the deformation temperature increases and the strain rate decreases. At the strain of 0.7, the η value is fluctuant within the range of 0.38~0.52, and the corresponding best processing parameters of hot deformation are the temperature range of 1040~1100 °C and the strain rate range of 0.01~0.14 s^{-1}. A better dynamic recrystallized microstructure may be obtained after the superalloy is deformed within the range of the process parameters.

In the power dissipation map, curvature change appears in the η value range of 0.32~0.38, and the corresponding processing parameters are in the temperature range of 1020~1040 °C and strain rate range of 0.01~0.08 s^{-1}; besides, curvature change appears in the contour of η under each strain. Since the γ' phase dissolves and consumes a part of the power in this temperature range, the power dissipation efficiency changes. This phenomenon also occurs in the hot processing map of other superalloys due to the internal phase transition or phase dissolution of the metallic material during hot deformation [19].

In order to verify the optimum process parameters obtained from the power dissipation map, the microstructure of the GH2907 superalloy corresponding to the highest value of η was observed. It can be seen from Fig.10 that as the deformation temperature increases and the strain rate decreases, the dynamic recrystallization phenomenon of the superalloy microstructure becomes more and more obvious. When the deformation temperature is 1100 °C and the strain rate is 0.01 s^{-1}, most original grains are replaced by dynamically recrystallized grains, and the microstructure softens, while some original grains are stretched. The growth of the crystal grains and uniformity of the superalloy microstructure are contributed by the higher deformation temperature, the smaller strain rate and the longer recrystallization time.

2.3.2 Hot processing map of GH2907 superalloy based on Prasad instability criteria

In the power dissipation map, the higher energy dissipation efficiency does not necessarily result in the better hot workability of the material. In the processing instability region, the materials may also have higher power dissipation efficiency[20]. If the system is unable to generate entropy at a rate above the strain rate applied to the system, the system will produce local rheology or rheological instability [21]. In order to avoid the occurrence of these unstable deformation mechanisms, the Prasad instability criterion was chosen to predict the deformation process parameters of the GH2907 superalloy during the hot deformation process.

Prasad's instability criterion is based on Ziegler's maximum entropy generation rate principle [22]. When dissipator co-content (J) and the strain rate satisfy the inequality Eq.(22) during the hot deformation of the metallic material, the rheological instability occurs.

$$\frac{\partial J}{\partial \dot{\varepsilon}} < \frac{J}{\dot{\varepsilon}} \tag{22}$$

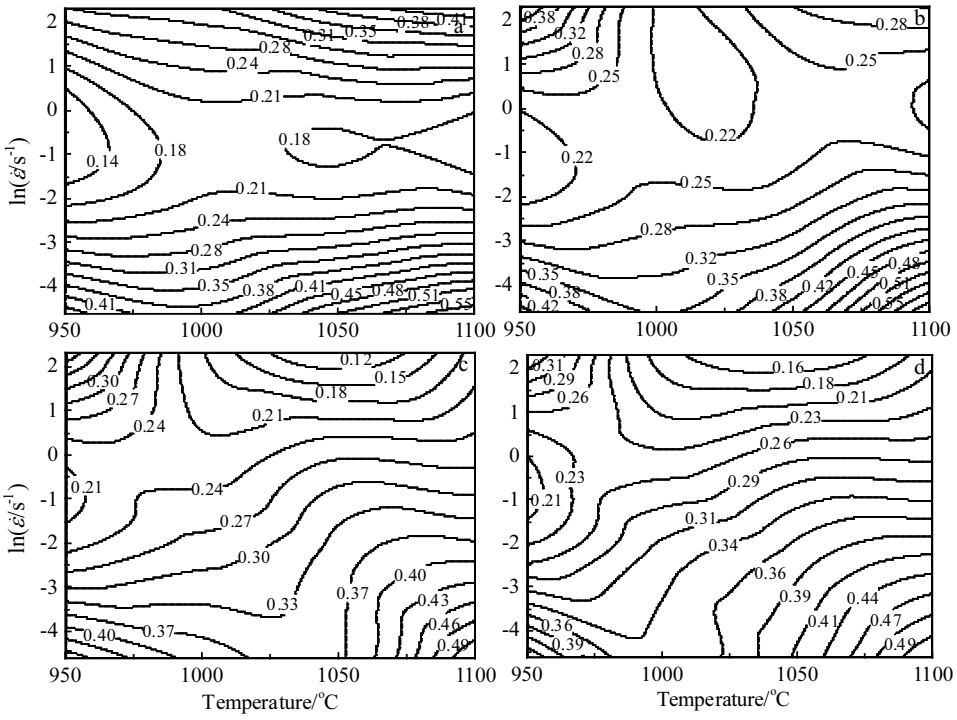

Fig.9 Power dissipation maps of GH2907 superalloy under different strain: (a) ε=0.1, (b) ε=0.3, (c) ε=0.5, and (d) ε=0.7

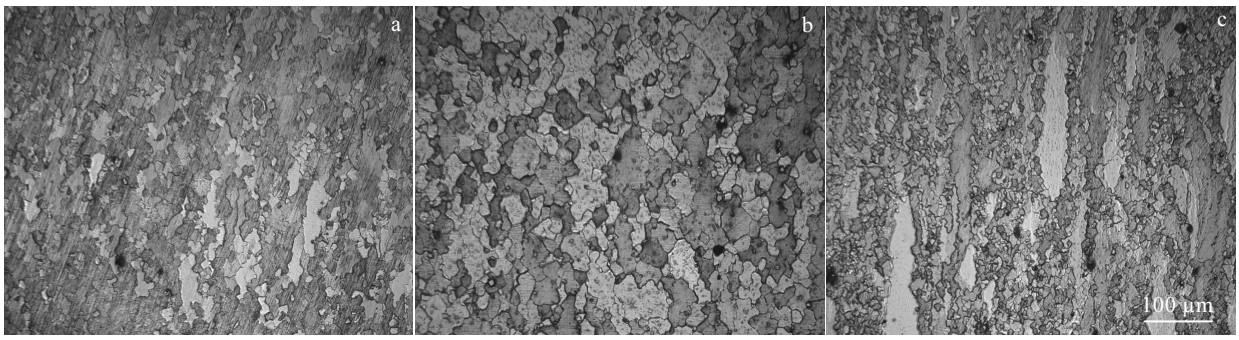

Fig.10 Microstructures of GH2907 superalloy under different deformation conditions: (a) 1050 °C/0.01 s^{-1}, (b) 1100 °C/0.01 s^{-1}, and (c) 1100 °C/0.1 s^{-1}

Eq.(15) and Eq.(22) are transformed into Eq.(23) and Eq.(24), respectively:

$$\frac{\partial \ln J}{\partial \ln \dot{\varepsilon}} = \frac{\partial \ln\left(\frac{m}{m+1}\right)}{\partial \ln \dot{\varepsilon}} + \frac{\partial \ln \sigma}{\partial \ln \dot{\varepsilon}} + 1 \tag{23}$$

$$\frac{\partial \ln J}{\partial \ln \dot{\varepsilon}} < 1 \tag{24}$$

Combining Eq.(22) and Eq.(23), the decision equation for the Prasad instability criterion can be derived:

$$\xi(\dot{\varepsilon}) = \frac{\partial \ln\left(\frac{m}{m+1}\right)}{\partial \ln \dot{\varepsilon}} + m < 0 \tag{25}$$

According to the strain rate sensitivity factor (m), the corresponding ln[m/(m+1)] is calculated, and the cubic spline interpolation function is used to establish the relationship between ln[m/(m+1)] and $\ln \dot{\varepsilon}$:

$$\ln\left(\frac{m}{m+1}\right) = b_1 + b_2 \ln \dot{\varepsilon} + 3b_3 \left(\ln \dot{\varepsilon}\right)^2 + b_4 \left(\ln \dot{\varepsilon}\right)^3 \tag{26}$$

A least squares cubic polynomial fitting is applied to the data, and the values of the coefficients b_1, b_2, b_3, and b_4 of the polynomial are obtained by regression. Deriving $\ln \dot{\varepsilon}$ on both sides of Eq.(26):

$$\frac{\partial \ln\left(\frac{m}{m+1}\right)}{\partial \ln \dot{\varepsilon}} = b_2 + 2b_3 \ln \dot{\varepsilon} + 3b_4 \left(\ln \dot{\varepsilon}\right)^2 \tag{27}$$

$$\xi(\dot{\varepsilon}) = b_2 + 2b_3 \ln \dot{\varepsilon} + 3b_4 \left(\ln \dot{\varepsilon}\right)^2 + m \tag{28}$$

The hot processing map (Fig.11) of GH2907 superalloy is established using Prasad instability criterion. When the strain is 0.1, the instability zone is located in the high temperature range of 1000~1040 °C and low strain rate range of 0.01~0.36 s^{-1}. When the strain is 0.3, the instability zones are located in the temperature range of 950~1030 °C and the strain rate range of 0.01~10 s^{-1} as well as 1080~1100 °C and 0.05~1 s^{-1}. As the strain increases, the instability zone moves toward the high temperature and high strain rate region as well as the low temperature and low strain rate region. When the strain is 0.7, the instability zone is located in the temperature range of 970~1100 °C and the strain rate range of 0.6~10 s^{-1}.

In the hot forming process of metallic materials, the main mechanisms causing deformation instability are adiabatic shear band, flow localization, fracture, rheological rotation, dynamic strain aging, etc [23]. According to the Prasad instability criterion, the instability zone of GH2907 superalloy during hot deformation is mainly concentrated in the high temperature and high strain rate region. In order to verify the accuracy of the Prasad instability criterion, the microstructure of the superalloy after the deformation parameters of the instability zone was observed.

The microstructure of the instability parameter obtained under the Prasad instability criterion is shown in Fig.12. The adiabatic shear band in the microstructure appears at the temperature of 1000 °C and strain rate of 1 s^{-1} as well as 1050 °C and 10 s^{-1}, while the flow localization in the microstructure is observed at the temperature of 1050 °C and strain rate of 1 s^{-1} as well as 1000 °C and 10 s^{-1}. The main reason for flow localization and adiabatic shear band appearance is that the heat which is generated in the thermal deformation process and cannot be diffused in the workpiece in time results in local temperature rise, and the deformation is more likely to occur in the high temperature region of the metallic materials [24]. The shear stress is the largest in the 45° direction to the axis during compression deformation and the material itself is less plastic, which contributes to the shear deformation in the 45° direction and adiabatic shear band occurrence. In addition, the angle between the adiabatic shear band and the direction of compression deformation is less than 45° generally for the continuous deformation. The deformation mechanism of flow localization is basically similar to that of adiabatic shear. The specimens are subjected to a certain degree of local deformation, and the strip-like microstructure generated by the flow localization is usually

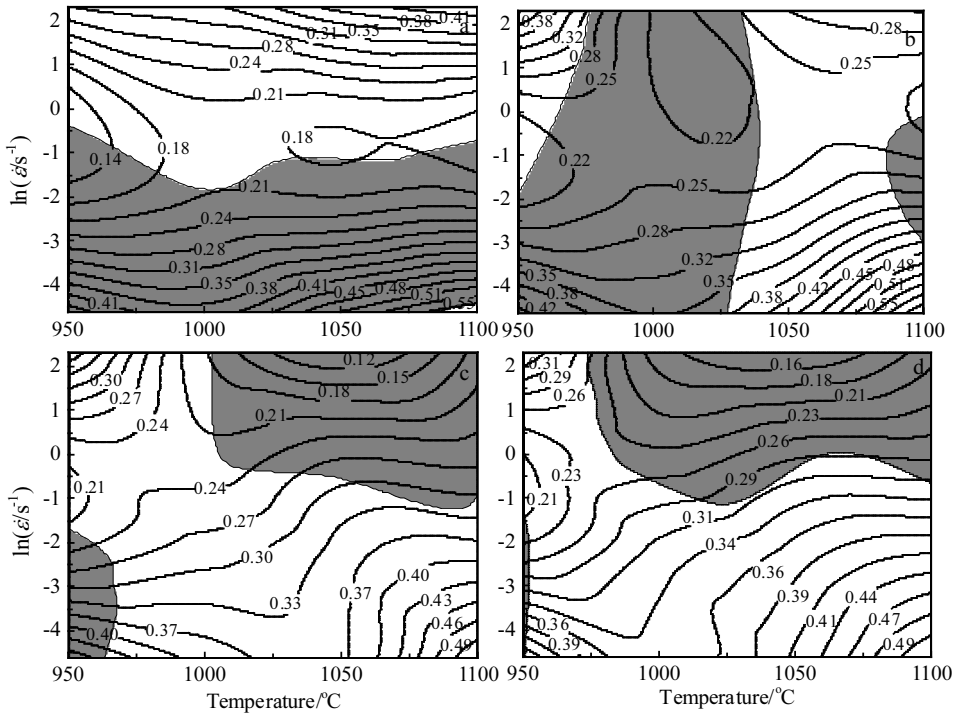

Fig.11 Processing maps of the GH2907 superalloy based on Prasad instability criterion under different strain: (a) ε=0.1, (b) ε=0.3, (c) ε=0.5, and (d) ε=0.7

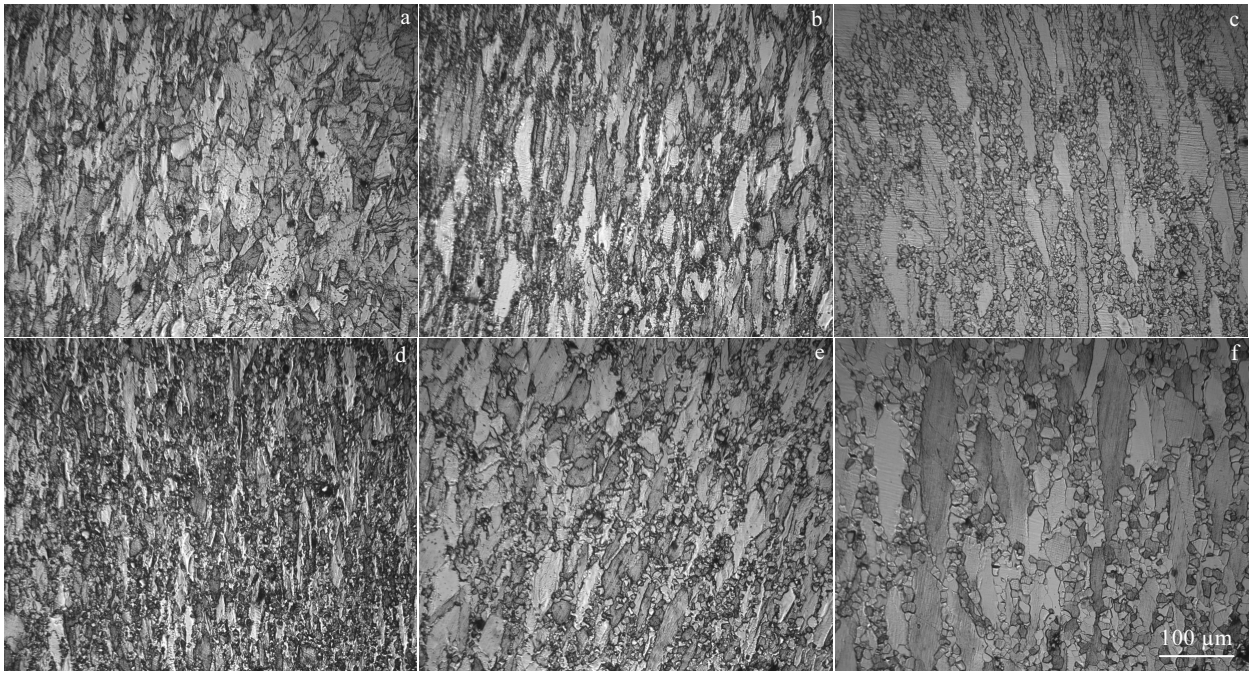

Fig.12 Microstructures of GH2907 superalloy after deformation at different deformation temperatures and strain rates: (a) 1000 °C/1 s^{-1}, (b) 1050 °C/1 s^{-1}, (c) 1100 °C/1 s^{-1}, (d) 1000 °C/10 s^{-1}, (e) 1050 °C/10 s^{-1}, and (f) 1100 °C/10 s^{-1}

about 35° to the main deformation direction. It can be seen that the uneven deformation in strip-like microstructure generated by flow localization is relatively weaker than that generated by adiabatic shear band. The adiabatic shear and flow localization phenomena gradually weaken and disappear as the deformation temperature increases and the strain rate decreases. Adiabatic shear deformation and flow localization which are thermoplastic instability phenomena of the material can be avoided in the actual deformation process through increasing the deformation temperature or reducing the strain rate.

3 Conclusions

1) The influence of deformation temperature and strain rate on the flow stress of GH2907 superalloy is analyzed. The flow stress decreases significantly with the decrease of strain rate or the increase of deformation temperature. The thermal deformation activation energy is calculated and the constitutive equation of GH2907 superalloy is established.

2) The power dissipation map of GH2907 superalloy under different strains is established. The region with large power dissipation efficiency (η) is located in the temperature range of 1050~1100 °C and the strain rate range of 0.01~0.03 s^{-1}. The microstructure under these process parameters has significant dynamic recrystallization.

3) The hot processing map of GH2907 superalloy is established. The instability zone obtained by Prasad instability criterion is concentrated in the high temperature range of 970~1100 °C and high strain rate range of 0.6~10 s^{-1}. The main mechanisms of the instability deformation of the superalloy are flow localization and adiabatic shear bands.

References

1 Lin Y C, Deng J, Jiang Y Q *et al*. *Materials Science and Engineering A*[J], 2014, 598: 251

2 Prasad Y. *Journal of Materials Engineering and Performance*[J], 2003, 12(6): 638

3 Yanagida A, Yanagimoto J. *Journal of Materials Processing Technology*[J], 2004, 151(1): 33

4 Chen F, Cui Z, Sui D *et al. Materials Science & Engineering A*[J], 2012, 528(15): 5073

5 Quan G Z, Li G S, Chen T *et al. Materials Science & Engineering A*[J], 2011, 528(13-14): 4643

6 Lin Y C, Chen M S, Zhong J. *Materials Letters*[J], 2008, 62(14): 2132

7 Huang S Y, Zhang S R, Li Dayong *et al. Transactions of Nonferrous Metals Society of China*[J], 2011, 21(8): 1817

8 Jiang H, Dong J, Zhang M *et al. Metallurgical and Materials Transactions A*[J], 2016, 47(10): 5071

9 McQueen H J, Ryan N D. *Materials Science and Engineering: A*[J], 2002, 322(1): 43

10 Zener C, Hollomon J H. *Journal of Applied Physics*[J], 1944, 15(1): 22

11 He A, Xie G, Zhang H *et al*. *Materials & Design*[J], 2013, 52: 677

12 Lin Y C, Chen M S, Zhong J. *Journal of Materials Processing Technology*[J], 2008, 205(1-3): 308

13 Imbert C, Mcqueen H. *Materials Science and Engineering A*[J], 2001, 313(1): 104

14 Ning Y, Fu M, Chen X. *Materials Science and Engineering A*[J], 2012, 540(1): 164

15 Quan G Z, Lv W Q, Mao Y P *et al. Materials & Design*[J], 2013, 50: 51

16 Song K, Aindow M. *Materials Science & Engineering A*[J], 2008, 479(1): 365

17 Zhang H, Zhang K, Lu Z *et al. Materials Science and Engineering A*[J], 2014, 604(16): 1

18 Solas D, Thébault Julien, Rey C *et al*. *Materials Science Forum*[J], 2010, 638-642: 2321

19 Ning Y, Yao Z, Li H, *et al. Materials Science and Engineering A*[J], 2010, 527(4): 961

20 Prasad Y V R K, Gegel H L, Doraivelu S M *et al. Metallurgical Transactions A*[J], 1984, 15(10): 1883

21 Chengcheng S, Shaosong J, Kaifeng Z. *Materials*[J], 2017, 10(12): 1437

22 Prasad Y, Seshacharyulu T. *International Materials Reviews*[J], 1998, 43(6): 243

23 Kodzhaspirov G E, Borowikow A, Terentyev M. *Materials Science Forum*[J], 2013, 762: 753

24 Ramanathan S, Karthikeyan R, Gupta M. *Journal of Materials Processing Technology*[J], 2007, 183(1): 104

GH2907 合金热变形行为及热加工图

陈益哲[1,2]，庞玉华[1,2]，王建国[3]，刘　东[3]，王健妍[4]

(1. 西安建筑科技大学，陕西 西安 710055)

(2. 陕西省冶金工程技术研究中心 陕西 西安 710055)

(3. 西北工业大学，陕西 西安 710072)

(4. 中国航发沈阳黎明航空发动机（集团）有限责任公司，辽宁 沈阳 110000)

摘　要：通过热模拟压缩实验研究了 GH2907 合金在变形温度为 950~1100 ℃、应变速率为 0.01~10 s^{-1}、变形量为 60%条件下的热变形行为。结果表明：流变应力随着变形温度的升高或应变速率的降低而显著降低；根据 Arrhenius 方程和 Zener-Hollomon 参数，计算了热变形激活能 Q，建立了 GH2907 合金的热变形本构方程；根据动态材料模型，确定了 GH2907 合金在不同应变下的功率耗散图，功率耗散效率 η 较高的区域位于温度为 1050~1100 ℃，应变速率为 0.01~0.03 s^{-1}，在该变形区域内组织发生了明显的动态再结晶现象；基于 Prasad 失稳判据，绘制了 GH2907 合金在不同应变下的热加工图，流变失稳区位于高温高应变速率区域，即温度为 970~1100 ℃，应变速率为 0.6~10 s^{-1} 范围，在该变形区域内动态再结晶晶粒沿着绝热剪切带且局部流动分布。根据 GH2907 合金热加工图及微观组织分析得到适宜的加工区域是温度 1050~1100 ℃，应变速率 0.01~0.03 s^{-1}。

关键词：GH2907合金；热变形行为；热加工图；功率耗散效率；失稳判据

作者简介：陈益哲，男，1992 年生，硕士生，西安建筑科技大学冶金工程学院，陕西 西安 710055，E-mail: 957698190@qq.com